CESifo WORKING PAPERS

9634
2022

March 2022

Impacts of Droughts and Floods on Agricultural Productivity in New Zealand as Measured from Space

Elodie Blanc, Ilan Noy

CESifo

Impressum:

CESifo Working Papers
ISSN 2364-1428 (electronic version)
Publisher and distributor: Munich Society for the Promotion of Economic Research - CESifo GmbH
The international platform of Ludwigs-Maximilians University's Center for Economic Studies and the ifo Institute
Poschingerstr. 5, 81679 Munich, Germany
Telephone +49 (0)89 2180-2740, Telefax +49 (0)89 2180-17845, email office@cesifo.de
Editor: Clemens Fuest
https://www.cesifo.org/en/wp
An electronic version of the paper may be downloaded
· from the SSRN website: www.SSRN.com
· from the RePEc website: www.RePEc.org
· from the CESifo website: https://www.cesifo.org/en/wp

CESifo *Working Paper No. 9634*

Impacts of Droughts and Floods on Agricultural Productivity in New Zealand as Measured from Space

Abstract

This study estimates the impact of excess precipitation (or the absence of rainfall) on productivity of agricultural land parcels in New Zealand. This type of post-disaster damage assessments aims to allow for quantification of disaster damage when on-the-ground assessment of damage is too costly or too difficult to conduct. It can also serve as a retroactive data collection tool for disaster loss databases where data collection did not happen at the time of the event. To this end, we use satellite-derived observations of terrestrial vegetation (the Enhanced Vegetation Index – EVI) over the growing season. We pair this data at the land parcel level identifying five land use types (three types of pasture, and annual and perennial crops) with precipitation records, which we use to identify both excessively dry and excessively wet episodes. Using regression analyses, we then examine whether these episodes of excess precipitation had any observable impact on agricultural productivity. Overall, we find statistically significant declines in agricultural productivity that is associated with both floods and droughts. The average impact of these events, averaged over the affected parcels, however, is not very large; usually less than 1%, but quite different across years and across regions. This average hides a heterogeneity of impacts, with some parcels experiencing a much more significant decline in the EVI.

JEL-Codes: Q150, Q540, C230.

Keywords: satellite-derived data, crop productivity, drought, flood.

*Elodie Blanc**
Massachusetts Institute of Technology (MIT)
Cambridge / MA / USA
eblanc@mit.edu

Ilan Noy
Victoria University of New Zealand
Wellington / New Zealand
ilan.noy@vuw.ac.nz

*corresponding author

1. Introduction

In the last few decades, satellite-based observations of terrestrial phenomena have been increasingly used for post-disaster damage assessments. Emergency responders, disaster risk managers, and scientists can use these data to obtain reliable information that can inform public policy.[1] This progress has been driven by technological advances in remote sensing that have led to a massive increase in temporal, spatial and spectral resolutions of satellite imagery and in the processing methods and computing power that are required to effectively interpret them.[2]

Satellite data are currently used for post-disaster damage assessment of various types of disasters caused by natural hazards, such as tropical cyclones, floods, earthquakes, landslides, and tsunamis. Most use daylight optical satellite data for post-disaster damage assessment, but some studies, such as,[3–5] utilized night-time light data to estimate hazard-induced electric power outages. For investigations of the impact of hazards on agriculture – the focus of this paper – only daylight imagery can be used.

Most optical satellite sensors gather surface reflectance data from the visible electromagnetic spectrum as well as emissivity data from the infrared wavelengths to produce images. Optical imagery is relatively easy to interpret as the resulting imagery typically appears as standard coloured or black and white photograph. The combination of visible and infrared wavelengths is particularly useful for the detection of water surfaces and vegetation-covered areas, and is therefore well suited for flood mapping or estimating storm- or flood-induced impacts on vegetation and agriculture. Vegetation "greenness" is typically estimated using various spectral indices such as the Normalized Difference Vegetation Index (NDVI), or the Enhanced Vegetation Index (EVI).[6] This last index is used in this study.

The applicability of optical satellite data for storm and flood damage assessment is partially limited due to its reliance on relatively cloud-free weather conditions for gathering the data and the fact that high precipitation is typically correlated with heavy cloud cover during the days surrounding the event. This constraint is especially relevant in tropical areas, where cloud cover is more common. While most of the previous research has focused on lower-income countries in the tropics where alternative data sources are rarely available, our focus is on a temperate country, New Zealand, where such issues are not as prevalent.

While New Zealand has institutions in place that could, in principle, collect ground data on disaster impacts, this is rarely done. Unlike in some other high-income countries, most agricultural production is not insured, so there is little reason for insurance companies (private or state-owned) to collect such data, and the state itself does not do so, either. Even in other temperate high-income countries, however, it is rare for insurance companies to share their data with the research community, so assessments of disaster damage and high spatial resolution are uncommon.

Remote sensing assessment is therefore a useful tool that should be added to the toolkit of post disaster assessments, not only in lower-income countries where they may be the only available option, but also for high-income countries, where the remote sensing data can be paired with other spatial data in order to improve the estimations of disaster damages. This coupling is often necessary because of various challenges in interpreting the remote imagery. Thus, combining the post-disaster remote sensing imagery with ancillary data such as satellite-derived Digital Elevation Models, static land use maps, and other datasets can be used to derive relevant information.

This is what we do in this paper. Our aim is to identify the impact of excess precipitation events (or its lack thereof) on productivity of agricultural land parcels. In a largely agricultural exporting country such as New Zealand, these extreme events (floods and droughts) may have quite a significant economic effect, which we aim to quantify. We do this by analysing the changes in the Enhanced Vegetation Index (EVI) over the growing season, and its correlation with episodes of excessive rainfall and its absence. We first identify, for each land parcel in the country, its growing season. We then calculate the peak EVI for each growing season for each land parcel as a measurement of agricultural productivity. We identify each land parcel by the crops growing on it using static agricultural census maps available from Land Information New Zealand (LINZ). We pair this data with the precipitation weather records, which we use to identify both excessively dry and excessively wet episodes during the growing cycle in each parcel. Using regression analysis, we then examine whether these episodes had any observable impact on agricultural productivity (as measured by the change in the EVI during the growing season).

Flood and storm damage assessments based on satellite imagery vary in their use of specific remote sensing sources and the corresponding spatial and temporal resolutions of the required imagery. High spatial, temporal, and spectral resolution imagery would often provide the most precise information, but it may not always be available. With respect to the spatial resolution, damage assessments are conducted on a range of available resolutions from low (>100 m/px) to moderate (5-100 m/px) and even high (<5 m/px) resolutions. For example, a study by Hoque et al.[7] used moderate resolution SPOT-5 imagery to analyse impacts of the 2007 Tropical Cyclone Sidr in Bangladesh. Phiri et al.[8] estimated the damages from the 2019 Cyclone Idai in Mozambique using moderate resolution Sentinel-2 images, Barnes et al.[9] used high resolution IKONOS imagery to estimate local damages of the 2005 Hurricane Katrina, and Mas et al.[10] studied the 2013 Typhoon Haiyan in the Philippines using images with similar resolution from Google Earth. For post-flood analysis, the publicly available Landsat images were utilized in damage assessments by Ma et al.[11], Li et al.[12], Hutanu et al.[13], and Sivanpillai et al.[14]. In some flood assessments, and as we do here, researchers combine satellite imagery with some ancillary data such as Digital Elevation Model maps[15–19]. MODIS data were used to estimate tropical storm damages to forests[20,21] and coastal vegetation[22]. Researchers also utilized moderate resolution Landsat or Sentinel-2 imagery to assess tropical storm impacts on coastal vegetation[23,24], forests[25], and mangroves[26,27].

Most of these studies focus on a particular disaster event, but Mandal and Hosaka[28] follow a different approach and assess long-run (29 years) impacts of cyclones on mangrove forests of India and Bangladesh based on Landsat and Google Earth imagery. Lu et al.[22] use MODIS data to estimate typhoon-induced vegetation damages in the southeast coastal region of China over a period of 18 years. Generally, these vegetation impact studies are estimated using spectral indices such as the NDVI, or the vegetation condition index (VCI).

Another subset of studies focuses on estimating storm and flood impacts on agriculture. Satellite-based flood crop loss assessments are typically conducted based on flood intensity, crop condition or a combination of these two methods[29]. Within this approach, crop damages are mostly estimated using stage-damage modelled damage curves based on satellite-derived criteria such as flood extent, duration, and timing. For tropical storm crop damage assessments, researchers used MODIS[30–32], Landsat[33] and SPOT-5[34].

Blanc and Strobl[35] used a combination of MODIS-derived data and typhoon-intensity measures generated from wind-field models to develop an algorithm for rice paddy typhoon damage

assessment. Omori et al.[31] similarly estimated cyclone damages to paddies also using MODIS data. Chejarla et al.[36] and Elodie et al. estimated cyclone economic loss for crops comparing vegetation biomass before and after the event. Moderate resolution SPOT-5 data are used by Chen and Lin[34] to assess typhoon impacts on agricultural lands and attempt to distinguish between damage caused by the wind and the heavy rainfall.

The studies mentioned above were mostly aimed at a general damage assessment for storm- or flood-affected areas. Several other studies focus specifically on analysing and quantifying damages to certain features of interest such as vegetation, forests, agricultural production, or buildings and infrastructure. Since our interest here is in rural floods and droughts, which generally do not have a very significant impact on buildings (at least in New Zealand), we limit the discussion here to damage to vegetation and consequently to agricultural production.

All these studies rely on detecting changes in the satellite images. This change detection is an automated algorithm aimed at detecting differences in images between two discrete points in time. Lu et al.[37] provides a review of 31 change detection approaches for remote sensing data such as image differencing (our approach), principal component analysis, post-classification comparison, unsupervised change detection and artificial neural networks.

Several studies analyse the efficacy of different change detection methods for tropical storm damage assessments. Several of these use a combination of object-based image analysis and a post-classification change detection method to estimate tropical storm impacts[8,38]. New change detection methods are being continuously developed to improve upon current approaches and enhance the efficiency of change detection for disaster damage assessment. Significant advances in machine learning algorithms suggest this field can still develop further (Zhu et al.[39]).

Overall, our study contributes in several ways: This is the first study that attempts to implement these approaches in the New Zealand context, with its rich land-use data at a very small scale (parcel level). We also use the long weather time-series that are available for New Zealand, these enable better identification of weather extremes (both excessive rainfall and drought). This availability of long time-series of weather data also enables us to focus on a longer time period, and not on single events as the vast majority of papers cited above do. Furthermore, the details available on land-use enable us to separately estimate the impact of droughts and floods on five different land use categories. This is important, as it is very likely, and as we indeed show, land use is important in determining the impact of flooding and droughts.

We note that our definition of flood events is based on identifying excess rainfall, as distinct from "the temporary covering of the soil surface by flowing water from any source including streams overflowing their banks, runoff from surrounding slopes and inflow from high tides" [40]. Ultimately, we estimate the effect of excess precipitation (flood) or its lack (drought), empirically, using a panel of the remotely obtained vegetation index data at the parcel boundary level.

2. Results

In the following subsections, we describe the impact of droughts and floods on crops (annual and perennial), and pasture (low yielding, with woody biomass, and high producing). For each, we present the regression results (equation 5), box plots that describe the impacts of floods and droughts over time (the annual growing seasons) and in each geographical region, and a series of maps that allows us to summarise these findings spatially.

Regression results are presented in Table 5 for annual crop and Table 6 for perennial crops, and for pasture in Tables 7-9 (for low-producing pastures, pastures with woody biomass, and high-producing pastures, respectively). The first two columns in each table present results including moderate or above droughts and floods (with and without control for whether the parcels are flood-prone). The next two columns provide the same for severe events (or above), and the last two for extreme events. In all regressions reported in tables 5-9, maximum and minimum temperatures are also included in their quadratic form.

In tables 5 and 6, floods and droughts have a negative impact on the productivity of both annual and perennial crops (as measured by the seasonal maximum of the EVI). The results for the temperature variables show, consistently for crops, that as minimum temperatures increase, crop productivity increases with a strengthening effect as the squared term is also positive and significant (though the linear term is non-significant in the case of perennial crops in table 6). For mean daily maximum temperatures, the effect is concave and always statistically significant, with the beneficial effect of higher temperatures tapering off as average maximum temperature increases.

In column (1), for both Tables 5 and 6, the flood and drought variables are both statistically significant and of comparable magnitude, except for floods for annual crops. For those, in Table 5, the coefficient is larger (3x), implying that floods damage annual crops more than they do perennial crops. Column (2) shows similar results to column (1), but with flood impacts distinguished between non-flood-prone areas and areas with a higher potential for flooding (i.e., flood return interval <60 years). For both types of crops, the effect of excess water is not necessarily larger in flood prone areas than in those with less flood risk when considering moderate and stronger events (statistically insignificant), but it is for severe and stronger event (statistically significant; see column (4)).

Overall, the main conclusions from Tables 5 and 6 are that indeed both floods and droughts damage annual and perennial crop productivity, and that this damage can be quantified using remote sensing data. For perennial crops (Table 6), the impact of flood-proness is more pronounced, but otherwise the results are quite similar.

Table 4 [Here]

Table 5 [Here]

The impacts of droughts and floods are presented in figure 5 and 6, for perennial and annual crops, respectively. These are presented by the specific extreme event effect, estimated using the coefficient estimates from column (1) of the regressions tables 5 and 6. These impacts are calculated as a proportion (in percentage term) of the long term average maximum EVI within a given plot. The box plots present the range of the plot level impacts of floods and droughts between the 25^{th} and 75^{th} percentiles across all regions by year in the top panel and across all years by region in the bottom graph. The lines inside the boxes represent the median values. The whiskers represent upper and lower adjacent values (i.e., 1.5 times the inter quartile range). Any values outside of the whiskers are omitted from the graphs.

Figure 5 [Here]

Figure 6 [Here]

The results in figure 5 show how some years have been worse, in terms of flood impacts on annual crops (e.g., 2008, 2011, and 2017) and some regions were, on average, more negatively affected by flooding events (e.g., Gisborne). These spatial and temporal patterns are repeated for perennial crops, but the impact seems to have been smaller (as measured by the EVI). For droughts, more adverse

years (as measured by declines in EVI) seems to have been 2015 and 2016 (for both perennial and annual crops). The variation across regions, especially with respect to the impacts of floods and droughts on perennial crops, appears to be less pronounced than it is for annual crops.

The maps in Figure 7 summarise the impact of each event type that is presented in Figure 5 and Figure 6 (drought/flood), averaged over the time period covered (2001-2017), and aggregated to the regional level. The patterns are quite different for droughts when compared to floods, and quite similar when comparing annual crops to perennial ones. For droughts, it is the eastern part of the South Island, and Taranaki and Northland in the North Island that had the steepest declines in the EVI as a consequence of droughts. For floods, the most impacted regions are Tasman in the South Island, and the eastern part of the North Island that are most vulnerable.

Figure 7 [Here]

Results for low-producing pastureland and the consequences of droughts and floods are presented using the same format as for crops in Table 7. Droughts and excess water are both detrimental to pasture growth. Pastureland in flood prone zones is additionally affected by excess rain. The effect is significantly stronger for all types of pasture when considering the effect in non-floodable areas (flood return period >60) and the flood prone zones. The only exception is for low producing pastures when considering extreme events only. In this specific case, the effect of excess rain is not significant in regions with no risk of flooding. As was the case for crops, we find little evidence that the set of more intense events (severe and extreme) is more damaging to pasture (as measured by the EVI) than the more moderate floods and droughts. It appears that most of the damage associated with these events is already incurred with the moderate flood and droughts events, so there does not seem to be much more incremental damage that is incurred when more intense extremes happen.

The effect of mean temperature on low-producing pasture differs somewhat from those observed for crops. For this type of pasture, the effects of both minimum and maximum temperature is concave, with the linear term always positive and significant, and the squared term always negative and significant.

Table 6 [Here]

The box plots representing the results in Table 6 are presented in Figure 8. Again, we see the expected variation over time, with some years experiencing a bigger adverse impact associated with floods and droughts (for example, 2015 for droughts and 2011 for floods). The bottom panel of Figure 8, and the map in Figure 11 presents the spatial distribution of the impact of floods and droughts on low-producing pasture. The spatial pattern is quite similar to the one we described for crops, with the eastern part of the South Island most vulnerable to droughts, and the eastern part of the North Island most vulnerable to floods, in terms of their impact on low-producing pasture.

Figure 8 [Here]

For pasture with woody biomass, we again observe similarly concave functions for both the minimum and maximum temperature. The results for the flood and drought indicators, in whatever severity they are measured, are also qualitatively identical to the ones we obtained when analysing low-productivity pasture. Both floods and droughts are damaging for agricultural productivity, as measured by the EVI, and for floods that impact is stronger in plots that are flood-prone (generally about twice as large). While there are some differences in the spatial distribution of impacts of floods and droughts on pasture with woody biomass, when compared to low-productivity pasture, these

differences are not very pronounced, and the general pattern (e.g., more flood impact in the eastern part of the North Island) still holds very clearly.

The results for high-producing pasture parcels, presented in Table 9 and Figure 10, are also quite similar to the other types of pasture (low-producing and with woody biomass). Even though these are sets of completely different pasture parcels, the results for the temperature variables are also quantitatively quite similar. However, in terms of the impact of the drought and flood variables, high-producing pasture seems to be more vulnerable to flood events than the other types of pasture, and the decline in the EVI observed there for the growing seasons with flood events is significantly larger (by a factor of 3-4). High-producing pasture, which is found in about twice as many parcels as low-producing pasture and pasture with woody biomass combined, is more vulnerable to floods. It is this type of pasture that is associated with the most significant decline in productivity as a result of flood events; it does not, however, seem to be more vulnerable to droughts than the other types of pasture (possibly because quite a lot of it is likely to be irrigated). The spatial distribution of these flood impacts (although of higher magnitude) is not dissimilar to what we find for the other types of pasture. Again, it is the eastern part of the North Island that is most vulnerable to flood events.

Table 7 [Here]

Table 8 [Here]

Figure 9 [Here]

Figure 10 [Here]

Figure 11 [Here]

3. Discussion

In the analysis presented here, we used satellite-based observations of terrestrial vegetation (the Enhanced Vegetation Index – EVI) in order to assess the impacts of floods and droughts. This is a type of post-disaster damage assessments which aims to allow for quantification of disaster damage when on-the-ground assessment of damage is too costly or too difficult to conduct, or needs to be conducted retroactively.

Satellite data have previously been used for post-disaster damage assessment of various types of disasters caused by natural hazards, such as tropical cyclones, floods, earthquakes, landslides, and tsunamis. Most use daylight optical satellite data (such as the MODIS images we use), but others have used night-time light data as well. The use of daylight optical satellite data for storm and flood damage assessment is often limited due to its reliance on relatively cloud-free weather conditions. This constraint is, however, especially relevant in tropical areas, and our focus is on a temperate country, New Zealand. Our second contribution to the literature relies on the availability of ancillary data that we use in conjunction with the remote sensing imagery. These are primarily high-resolution land use maps, detailed weather records (both temperature and precipitation), and data on irrigation.

Overall, we find statistically significant declines in agricultural productivity that is associated with both floods and droughts, and identified in all the five types of land uses we examine – three types of pasture, and annual and perennial crops. However, the average impact of these events, averaged over the affected parcels, is not very large; usually less than 1%, but it is quite different across years and across regions. This average hides a heterogeneity of impacts, with some parcels experiencing a much more significant decline in the EVI.

These declines we identified, however, may not imply financial losses to farm businesses. Pourzand et al.[68], for example, has shown that droughts have not caused a dramatic decrease in the profitability of dairy farms over the past two decades in New Zealand. This is likely the case because, as we document here, agricultural production in New Zealand seems to be, still, quite resilient to these shocks. It is also most likely caused because droughts and floods may change market prices in ways that ameliorate their impact on farm revenue and profitability (given the negative supply shock, prices rise). As such, market changes may be obscuring some of the adverse wellbeing impact that are caused by these climatic events, as the purchasing power of the consumers of these agricultural products are the ones bearing the burden of these events' impacts.

Overall, we argue that remote sensing assessment is a useful tool that should be added to the toolkit of post disaster assessments and the construction and collection of disaster loss databases. Furthermore, combining post-disaster remote sensing imagery with ancillary data can provide information about disaster impacts that is not otherwise available and can serve to inform policy that aims to mitigate or ameliorate the impact of these events.

4. Methods

4.1. Data

The dataset used to estimate the impact of flood on land productivity is constructed at the parcel level and provides information on the land use type, vegetation, growing seasons, and weather.

4.1.1. Parcels boundaries

To determine plot boundaries, we use NZ primary parcels polygons available from Land Information New Zealand (LINZ). This data is publicly available for download at https://data.linz.govt.nz/layer/50772-nz-primary-parcels/. LINZ defines a primary parcel as "a portion of land that is intended to be: owned by the Crown, except moveable marginal strips; Held in fee simple (predominately private ownership); Maori freehold land or Maori customary land; Public foreshore and seabed; The bed of a lake or river; Road or Railway; Vested in a local authority." The layer has a nominal accuracy of 0.1 to 1m in urban areas and 1 to 100m in rural areas. For the purpose of this study, we excluded parcels classified as 'public foreshore and seabed', 'bed of a lake or river', and 'road or railway'.

4.1.2. Land use

To determine land use within each parcel, we used information from the Land Use Carbon Analysis (LUCAS) land use map (v. 008) developed by the New Zealand Ministry for the Environment. Available for download at https://data.mfe.govt.nz/layer/52375-lucas-nz-land-use-map-1990-2008-2012-2016-v008/. The LUCAS land use map use a range of remote sensing, environmental and land use data sources to distinguish 12 land use classes over New Zealand, including three forest classes (Pre-1990 natural forest, Pre-1990 planted forest, and Post-1989 forest), two classes of grassland (high-producing and low-producing woody biomass), and two classes of cropland (perennial and annual). For some of these classes, subclasses are also defined (e.g. for high and low producing cropland, five sub-classes are distinguished: unknown, winter forage, grazed – dairy, grazed - non-dairy, and ungrazed). We do not use these sub-classifications when producing our empirical estimates.

We remove from our dataset all parcels with non-agricultural uses (wetland, settlement and others), as defined in the LUCAS land use maps, and keep only forests, grassland and cropland. Land use information is available for 1 January 1990, 1 January 2008, 31 December 2012 and 31 December 2016. We consider that for a given year, the land use type corresponds to 2008 land use for the years up to 2010, the 2012 land use for the period from 2011 to 2013, and the 2016 land use for the period 2014 and after. Each of these land use types is associated with a primary parcel. If a parcel has multiple land uses, the parcel will be sub-divided into as many parts as there is land use classes.

Figure 1 [Here]

4.1.3. Vegetation indices

To represent vegetation growth, we extracted satellite derived imagery of vegetation indices. We use the images from Terra Moderate Resolution Imaging Spectroradiometer (MODIS) Vegetation Indices (MOD13Q1) Version 6, which is provided every 16 days at a 250m resolution (these data are available for download at https://lpdaac.usgs.gov/products/mod13q1v006/). Two indices are available: the Normalized Difference Vegetation Index (NDVI), and the Enhanced Vegetation Index (EVI), which has improved sensitivity over high biomass regions. Cloudy and low-quality pixels are masked. NDVI is calculated using the near-infrared (NIR) and red spectral bands reflectance ρ:

$$NDVI = \frac{\rho_{NIR} - \rho_{red}}{\rho_{NIR} + \rho_{red}} \quad (1)$$

EVI reduces residual atmospheric contamination and variable soil back-ground reflectance by adjusting the reflectance in the red band as a function of the reflectance in the blue band. It is often also used where the leaf area index is high in order to improve the accuracy of the NDVI:

$$EVI = 2.5 \frac{\rho_{NIR} - \rho_{red}}{\rho_{NIR} + 6\rho_{red} - 7.5\rho_{blue} + 1} \quad (2)$$

Figure 2 [Here]

4.1.4. Growing season

To determine the growing season, we use the MODIS Global Land Cover Dynamics Product (MCD12Q2) Version 6 (these data are available for download at https://lpdaac.usgs.gov/products/mcd12q2v006/). This product records annually since 2001 at a 500m resolution vegetation phenology metrics such as greenness increase and peak, senescence, and dormancy, which characterizes vegetation growth cycles. An algorithm is used to determine the timing of phenometrics which are derived from time series of MODIS adjusted surface reflectances EVI (NBAR-EVI2). The start of the growing season is characterized by the greenup onset (when EVI2 first crossed 15% of the segment EVI2 amplitude), and the end by the onset of dormancy (when EVI2 last crossed 15% of the segment EVI2 amplitude). Up to two vegetation cycles are detected to account for multi-cropping.

For the purpose of this study, which spans from 2000 to 2015, we have calculated the average growing season for each property and land use, and associated this average growing seasons also to the first year of the sample, for which MCD12Q2 data were not available.

4.1.5. Climate

To calculate the incidence of droughts and floods on vegetation, we first consider the Standardised Precipitation Index (SPI). This measure is commonly used to represent the effect of precipitation over regions characterised by multiple climatic zones as it represents a standardized departure from the mean of a long-term trend [41]. The SPI is calculated by first fitting a gamma probability density function to the frequency distribution of rainfall over a reference period (of at least 30 years), which is then used to determine the cumulative probability of a particular precipitation level for a chosen time scale and finally transformed into a normal distribution ~N(0,1)[42]. SPI values are therefore expressed in terms of standard deviations from the median. Negative values imply below normal precipitations, while positive values indicate above normal rainfall. Using the SPI, it is possible to identify periods of drought (McKee et al., 1993) and floods [43]. A moderate drought starts when the SPI falls below 0 and ends when the index returns to a positive value after reaching a value of –1. Floods are calculated

similarly with a threshold of +1. The thresholds for severe and extreme droughts or floods are identified with thresholds of +/-1.5 and +/-2, respectively. Time scales of 1 to 48 months can be used to calculate the SPI depending on the responsivity of the sector considered (meteorologic, agricultural, hydrologic, and socio-economic). For instance, longer scales are more suitable for water resources management (e.g., for reservoirs), while shorter time scales are better suited at detecting drought events affecting agriculture, especially for areas that are not irrigated[44]. Statistical analyses of the impact of droughts on crops have used scales from 3 to 12 months[12,30,45–47]. In this study, SPI is calculated on a 2-, 3- and 6-months' time scales, using 1972-2005 as a reference period.

Following McKee et al.[42], we also calculate the magnitude of a drought (*DM*), which is:

$$DM = \frac{-(\sum_{j=m}^{x} SPI_j)}{GSlength} \quad (3)$$

where *m* is the starting month of the drought and *x* is the end of the drought. For the purpose of this study, *x* corresponds to either the end of the drought or the end of the growing season, whichever occurs first within the same growing season. To account for the effect of the growing season duration, the magnitude is taken as ratio of *GSlentgh*. Similarly, the magnitude of a flood (*FM*) is calculated as:

$$FM = \frac{(\sum_{j=m}^{x} SPI_j)}{GSlength} \quad (4)$$

Precipitation data used to calculate the flood occurrences, are extracted from the Virtual Climate station Network (VCSN) database available from the National Institute of Water and Atmospheric Research (NIWA). Those data are available daily at a 5km resolution. Daily minimum and maximum diurnal temperatures are also obtained from the VCSN, and based on these, we also calculate the mean daily temperature as: $Tmean = (Tmin + Tmax)/2$.

Figure 3 [Here]

4.1.6. Flood return interval

The SPI measures precipitation rather than physical flooding. Therefore, information on soil physical attributes is necessary to estimate the effect of excess precipitation on plant productivity. To this end, we use the flood return interval from the New Zealand Fundamental Soil Layer which represents the probability of flooding (this data is available for download at https://lris.scinfo.org.nz/layer/48106-fsl-flood-return-interval/). This delineation of land at risk of flooding provides a proxy for physical attributes such as slope, catchment area, surface permeability, etc, which play a role in how excessive rainfall would affect plants. However, as a full hydrological modelling of flooding throughout New Zealand is beyond the scope of this project, the flood return interval are characterized by six classes described in Webb & Wilson[40] (for built property and infrastructure, those risk classes are quite moderate. In many places, a 'flood prone' house is defined as one that is exposed to a 1 in 100 years flooding event).

A map of the flood return interval in NZ is provided in Figure 4 and shows that most of the land in NZ is not regularly affected by floods. To match flooding risk at the parcel level, we attribute the flood return interval class the most common to each plot.

Figure 4 [Here]

4.1.7. Sample description and summary statistics

The short name and description of the variables used in the analysis are described in Table 1. Summary statistics for those variables are provided in Table 3 for crops and Table 4 for pasture.

Table 1 [Here]

By construction, as a severe event is included in the 'moderate and above' category, a 'moderate and above' has a higher magnitude than the 'severe and stronger' category.

Table 2 [Here]

Table 3 [Here]

4.2. Methods

As a measure of crop yields, one can use a vegetation index. Vegetation indices, such as the Normalized Difference Vegetation Index (NDVI), have been used in the past two decades to proxy crop productivity. They provide a consistent spatial and temporal representation of vegetation conditions. Numerous studies have demonstrated that NDVI values are significantly correlated with yields of crop such as wheat[48–54], sorghum [55], corn [56,57], rice [54,58,59], soybean [57], barley [60], millet [61] and tomato [62].

The Enhanced Vegetation Index (EVI) has been used more recently, as it is more responsive to variation in vegetation canopy structures compared to NDVI [63]. Studies have shown a significant correlation between the EVI and the yield of corn [64] and rice [65]. Previous research, considering an ensemble of ten globally significant crops, and found that the EVI shows better correlation with crop yields overall, than the NDVI [66]. We therefore focused on the EVI only and considered its maximum value within the growing season to be representative of crop productivity within that season. See Shammi and Meng [67], for example, for the use of the season's peak reading of EVI as a good indicator of crop yields.

The base regression specification was formulated as follows:

$$EVI_{pt}^{max} = \alpha + \beta_1 T_{pt}^{min} + \beta_2 (T_{pt}^{min})^2 + \beta_3 T_{pt}^{max} + \beta_4 (T_{pt}^{max})^2 + \beta_5 D_{pt} + \beta_6 F_{pt} + \mu_p + \varepsilon_{pt} \qquad (5)$$

where EVI_{pt}^{max} is the maximum observed peak EVI during the growing season in plot (*p*) and growing season year (*t*), T_{pt}^{min} and T_{pt}^{max} are the average minimum and maximum diurnal temperature over the growing season in the same plot/year combination; and their square terms are also included. *D* is the drought binary indicator (as described above), *F* is the flood indictor. μ is a plot fixed-effect to account for plot-specific time-invariant differences in plant productivity, and ε is the error term.

The droughts and flood indicators are calculated using different thresholds that represent either moderate, severe, or extreme events. To separate the effect of excess water on crops located in flood prone area (versus land that is not prone to periodic flooding), we also added to these specifications an interaction term between flood variables and the *rf2345* flood-zone variable that is described above.

We also considered the effect of irrigation and the expected lessening of the effect of drought on productivity that irrigation may generate. However, data on irrigation are only available at the parcel level for the years 2017 and 2020. These data are available for download athttps://data.mfe.govt.nz/layer/90838-irrigated-land-area-2017/ for 2017 and https://data.mfe.govt.nz/layer/105407-irrigated-land-area-raw-2020-update/ for 2020. They are available at the subregional level for 2002 and 2017. These data are available for download at https://data.mfe.govt.nz/layer/99907-irrigated-land-area-grid-aps-2002/ for 2002 and https://data.mfe.govt.nz/layer/99908-irrigated-land-area-grid-aps-2017/ for 2017. None of these

irrigation data provided reasonable results, most likely due to the sparse time and spatial coverage of the data and the significant changes in irrigation systems in the last two decades.

We also estimated specifications representing non-linear effects of temperature using fractional polynomial, but results were very similar to the reported quadratic specifications, so the more parsimonious quadratic approach was preferred.

References

1. Voigt, S. *et al.* Global trends in satellite-based emergency mapping. *Science* **353**, 247–252 (2016).

2. Notti, D. *et al.* Potential and Limitations of Open Satellite Data for Flood Mapping. *Remote Sens. 2018, Vol. 10, Page 1673* **10**, 1673 (2018).

3. Molthan, A. & Jedlovec, G. Satellite observations monitor outages from superstorm sandy. *Eos (Washington. DC).* **94**, 53–54 (2013).

4. Román, M. O. *et al.* Satellite-based assessment of electricity restoration efforts in Puerto Rico after Hurricane Maria. *PLoS One* **14**, e0218883 (2019).

5. Sarkar, S. Rapid assessment of cyclone damage using NPP-VIIRS DNB and ancillary data. *Nat. hazards (Dordrecht, Netherlands)* **106**, 579–593 (2021).

6. Fayne, J., Bolten, J., Lakshmi, V. & Ahamed, A. Optical and Physical Methods for Mapping Flooding with Satellite Imagery. 83–103 (2017) doi:10.1007/978-3-319-43744-6_5.

7. Hoque, M. A. A., Phinn, S., Roelfsema, C. & Childs, I. Assessing tropical cyclone impacts using object-based moderate spatial resolution image analysis: a case study in Bangladesh. *Int. J. Remote Sens.* **37**, 5320–5343 (2016).

8. Phiri, D., Simwanda, M. & Nyirenda, V. Mapping the impacts of cyclone Idai in Mozambique using Sentinel-2 and OBIA approach. *South African Geogr. J.* **103**, 237–258 (2021).

9. Barnes, C. F., Fritz, H. & Yoo, J. Hurricane disaster assessments with image-driven data mining in high-resolution satellite imagery. *IEEE Trans. Geosci. Remote Sens.* **45**, 1631–1640 (2007).

10. Mas, E. *et al.* Field survey report and satellite image interpretation of the 2013 Super Typhoon Haiyan in the Philippines. *Nat. Hazards Earth Syst. Sci.* **15**, 805–816 (2015).

11. Ma, Y., Liu, X., Li, X., Sun, Y. & Li, X. Rapid assessment of flood disaster loss in Sind and Punjab province, Pakistan based on RS and GIS. *2011 Int. Conf. Multimed. Technol. ICMT 2011* 646–649 (2011) doi:10.1109/ICMT.2011.6003024.

12. Li, S. *et al.* Automatic near real-time flood detection using Suomi-NPP/VIIRS data. *Remote Sens. Environ.* **204**, 672–689 (2018).

13. Hutanu, E., Urzica, A. & Enea, A. Evaluation of Damages Caused by Floods, Based on Satellite Images. Case Study: Jijia River, Slobozia-Dângeni Sector, July 2010. *Present Environ. Sustain. Dev.* **12**, 135–146 (2018).

14. Sivanpillai, R., Jacobs, K. M., Mattilio, C. M. & Piskorski, E. V. Rapid flood inundation mapping by differencing water indices from pre- and post-flood Landsat images. *Front. Earth Sci. 2020 151* **15**, 1–11 (2020).

15. Gianinetto, M., Villa, P. & Lechi, G. Postflood damage evaluation using Landsat TM and ETM+ data integrated with DEM. *IEEE Trans. Geosci. Remote Sens.* **44**, 236–243 (2006).

16. Lamovec, P., Mikos, M. & Ostir, K. Detection of flooded areas using machine learning techniques: Case study of the Ljubljana moor floods in 2010. *Disaster Adv.* **6**, 4–11 (2013).

17. Lamovec, P., Veljanovski, T., Mikoš, M. & Oštir, K. Detecting flooded areas with machine learning techniques: case study of the Selška Sora river flash flood in September 2007. *https://doi.org/10.1117/1.JRS.7.073564* **7**, 073564 (2013).

18. Franci, F., Boccardo, P., Mandanici, E., Roveri, E. & Bitelli, G. Flood mapping using VHR satellite imagery: a comparison between different classification approaches. *https://doi.org/10.1117/12.2241390* **10005**, 46–54 (2016).

19. Malinowski, R. *et al.* Detection and Delineation of Localized Flooding from WorldView-2 Multispectral Data. *Remote Sens. 2015, Vol. 7, Pages 14853-14875* **7**, 14853–14875 (2015).

20. Wang, F. & Xu, Y. J. Comparison of remote sensing change detection techniques for assessing hurricane damage to forests. *Environ. Monit. Assess.* **162**, 311–326 (2010).

21. Rossi, E., Rogan, J. & Schneider, L. Mapping forest damage in northern Nicaragua after Hurricane Felix (2007) using MODIS enhanced vegetation index data. *http://dx.doi.org/10.1080/15481603.2013.820066* **50**, 385–399 (2013).

22. Lu, L., Wu, C. & Di, L. Exploring the Spatial Characteristics of Typhoon-Induced Vegetation Damages in the Southeast Coastal Area of China from 2000 to 2018. *Remote Sens. 2020, Vol. 12, Page 1692* **12**, 1692 (2020).

23. Rodgers, J. C., Murrah, A. W. & Cooke, W. H. The impact of hurricane katrina on the coastal vegetation of the weeks bay reserve, alabama from NDVI data. *Estuaries and Coasts* **32**, 496–507 (2009).

24. Charrua, A. B., Padmanaban, R., Cabral, P., Bandeira, S. & Romeiras, M. M. Impacts of the Tropical Cyclone Idai in Mozambique: A Multi-Temporal Landsat Satellite Imagery Analysis. *Remote Sens. 2021, Vol. 13, Page 201* **13**, 201 (2021).

25. Zhang, X., Wang, Y., Jiang, H. & Wang, X. Remote-sensing assessment of forest damage by Typhoon Saomai and its related factors at landscape scale. *http://dx.doi.org/10.1080/01431161.2013.827344* **34**, 7874–7886 (2013).

26. Bhowmik, A. K. & Cabral, P. Cyclone Sidr Impacts on the Sundarbans Floristic Diversity. *Earth Sci. Res.* **2**, (2013).

27. Hu, T. & Smith, R. The Impact of Hurricane Maria on the Vegetation of Dominica and Puerto Rico Using Multispectral Remote Sensing. *Remote Sens.* **10**, 827-undefined (2018).

28. Mandal, M. S. H. & Hosaka, T. Assessing cyclone disturbances (1988–2016) in the Sundarbans mangrove forests using Landsat and Google Earth Engine. *Nat. Hazards* **102**, 133–150 (2020).

29. Rahman, M. S. & Di, L. A Systematic Review on Case Studies of Remote-Sensing-Based Flood Crop Loss Assessment. *Agric. 2020, Vol. 10, Page 131* **10**, 131 (2020).

30. Blanc, É. & Strobl, E. The impact of climate change on cropland productivity: evidence from satellite based products at the river basin scale in Africa. *Clim. Change* **117**, 873–890 (2013).

31. Omori, K. *et al.* Assessment of paddy fields' damage caused by Cyclone Nargis using MODIS time-series images (2004–2013). *Paddy Water Environ.* **19**, 271–281 (2021).

32. Cortés-Ramos, J., Farfán, L. M. & Herrera-Cervantes, H. Assessment of tropical cyclone damage on dry forests using multispectral remote sensing: The case of Baja California Sur, Mexico. *J. Arid Environ.* **178**, 104171 (2020).

33. Goto, K., Goto, T., Nmor, J. C., Minematsu, K. & Gotoh, K. Evaluating salinity damage to crops through satellite data analysis: application to typhoon affected areas of southern Japan. *Nat. Hazards* **75**, 2815–2828 (2015).

34. Chen, T. H. & Lin, K. H. E. Distinguishing the windthrow and hydrogeological effects of typhoon impact on agricultural lands: an integrative OBIA and PPGIS approach. *https://doi.org/10.1080/01431161.2017.1382741* **39**, 131–148 (2017).

35. Blanc, É. & Strobl, E. Assessing the Impact of Typhoons on Rice Production in the Philippines. *J. Appl. Meteorol. Climatol.* **55**, 993–1007 (2016).

36. Chejarla, V. R., Mandla, V. R., Palanisamy, G. & Choudhary, M. Estimation of damage to agriculture biomass due to Hudhud cyclone and carbon stock assessment in cyclone affected areas using Landsat-8. *http://dx.doi.org/10.1080/10106049.2016.1161079* **32**, 589–602 (2016).

37. Lu, D. *et al.* Change detection techniques. *https://doi.org/10.1080/0143116031000139863* **25**, 2365–2401 (2010).

38. Hoque, M., Phinn, S., Roelfsema, C. & Childs, I. Assessing tropical cyclone damage using moderate spatial resolution satellite imagery: Cyclone Sidr, Bangladesh 2007. in *ACRS 2015 - 36th Asian Conference on Remote Sensing: Fostering Resilient Growth in Asia, Proceedings* (Philippine Geosciences and Remote Sensing Societyand Asian Association on Remote Sensing, 2015).

39. Zhu, X. X. *et al.* Deep Learning in Remote Sensing: A Comprehensive Review and List of Resources. *IEEE Geosci. Remote Sens. Mag.* **5**, 8–36 (2017).

40. Webb, Thr. & Wilson, A. *A manual of land characteristics for evaluation of rural land*. *Landcare Research Science Series 10* (1995).

41. Jones, P. D. & Hulme, M. Calculating regional climatic time series for temperature and precipitation: methods and illustrations. *Int. J. Climatol.* **16**, 361–377 (1996).

42. McKee, T. B., Doesken, N. J. & Kleist, J. The Relationship of Drought Frequency and Duration to Time Scales. in *8th Conference on Applied Climatology, California* 179–184 (1993).

43. Seiler, R. A., Hayes, M. & Bressan, L. Using the standardized precipitation index for flood risk monitoring. *Int. J. Climatol.* **22**, 1365–1376 (2002).

44. McKee, T. B. & Edwards, D. C. *Characteristics of 20th century drought in the United States at Multiple Time Scales*. *Atmospheric Science Paper 634, Climatology Report 97-2* https://mountainscholar.org/handle/10217/170176 (1997).

45. Feng, P. *et al.* Impacts of rainfall extremes on wheat yield in semi-arid cropping systems in eastern Australia. *Clim. Change* **147**, 555–569 (2018).

46. Hoffman, A. L., Kemanian, A. R. & Forest, C. E. Analysis of climate signals in the crop yield record of sub-Saharan Africa. *Glob. Chang. Biol.* **24**, 143–157 (2017).

47. Yamoah, C. F., Walters, D. T., Shapiro, C. A., Francis, C. A. & Hayes, M. J. Standardized precipitation index and nitrogen rate effects on crop yields and risk distribution in maize. *Agric. Ecosyst. Environ.* **80**, 113–120 (2000).

48. Das, D. K., Mishra, K. K. & Kalra, N. Assessing growth and yield of wheat using remotely-sensed canopy temperature and spectral indices. *https://doi.org/10.1080/01431169308904421* **14**, 3081–3092 (2007).

49. Doraiswamy, P. C. & Cook, P. W. Spring Wheat Yield Assessment Using NOAA AVHRR Data. *http://dx.doi.org/10.1080/07038992.1995.10874595* **21**, 43–51 (2014).

50. Gupta, R. K., Prasad, S., Rao, G. H. & Nadham, T. S. V. District level wheat yield estimation using NOAA/AVHRR NDVI temporal profile. *Adv. Sp. Res.* **13**, 253–256 (1993).

51. Hochheim, K. P. & Barber, D. G. Spring Wheat Yield Estimation for Western Canada Using NOAA NDVI Data. *https://doi.org/10.1080/07038992.1998.10874687* **24**, 17–27 (2014).

52. Labus, M. P., Nielsen, G. A., Lawrence, R. L., Engel, R. & Long, D. S. Wheat yield estimates using multi-temporal NDVI satellite imagery. *https://doi.org/10.1080/01431160110107653* **23**, 4169–4180 (2010).

53. Lopresti, M. F., Di Bella, C. M. & Degioanni, A. J. Relationship between MODIS-NDVI data and wheat yield: A case study in Northern Buenos Aires province, Argentina. *Inf. Process. Agric.* **2**, 73–84 (2015).

54. Guan, S. *et al.* Assessing Correlation of High-Resolution NDVI with Fertilizer Application Level and Yield of Rice and Wheat Crops Using Small UAVs. *Remote Sens. 2019, Vol. 11, Page 112* **11**, 112 (2019).

55. Potdar, M. B. Sorghum yield modelling based on crop growth parameters determined from visible and near-IR channel NOAA AVHRR data. *http://dx.doi.org/10.1080/01431169308904385* **14**, 895–905 (2007).

56. Hayes, M. J. & Decker, W. L. Using NOAA AVHRR data to estimate maize production in the United States Corn Belt. *http://dx.doi.org/10.1080/01431169608949138* **17**, 3189–3200 (2007).

57. Prasad, A. K., Chai, L., Singh, R. P. & Kafatos, M. Crop yield estimation model for Iowa using remote sensing and surface parameters. *Int. J. Appl. Earth Obs. Geoinf.* **8**, 26–33 (2006).

58. Quarmby, N. A., Milnes, M., Hindle, T. L. & Silleos, N. The use of multi-temporal NDVI measurements from AVHRR data for crop yield estimation and prediction. *http://dx.doi.org/10.1080/01431169308904332* **14**, 199–210 (2007).

59. Nuarsa, I. W., Nishio, F., Nishio, F., Hongo, C. & Hongo, C. Relationship between Rice Spectral and Rice Yield Using Modis Data. *J. Agric. Sci.* **3**, p80 (2011).

60. Weissteiner, C. J. & Kühbauch, W. Regional Yield Forecasts of Malting Barley (Hordeum vulgare L.) by NOAA-AVHRR Remote Sensing Data and Ancillary Data. *J. Agron. Crop Sci.* **191**, 308–320 (2005).

61. Groten, S. M. NDVI—crop monitoring and early yield assessment of Burkina Faso. *http://dx.doi.org/10.1080/01431169308953983* **14**, 1495–1515 (2007).

62. Koller, M. & Upadhyaya, S. K. Prediction of Processing Tomato Yield Using a Crop Growth Model and Remotely Sensed Aerial Images. *Trans. ASAE* **48**, 2335–2341 (2005).

63. Huete, A. *et al.* Overview of the radiometric and biophysical performance of the MODIS vegetation indices. *Remote Sens. Environ.* **83**, 195–213 (2002).

64. Bolton, D. K. & Friedl, M. A. Forecasting crop yield using remotely sensed vegetation indices and crop phenology metrics. *Agric. For. Meteorol.* **173**, 74–84 (2013).

65. Son, N. T., Chen, C. F., Chen, C. R., Minh, V. Q. & Trung, N. H. A comparative analysis of multitemporal MODIS EVI and NDVI data for large-scale rice yield estimation. *Agric. For. Meteorol.* **197**, 52–64 (2014).

66. Johnson, D. M. A comprehensive assessment of the correlations between field crop yields and commonly used MODIS products. *Int. J. Appl. Earth Obs. Geoinf.* **52**, 65–81 (2016).

67. Shammi, S. A. & Meng, Q. Use time series NDVI and EVI to develop dynamic crop growth metrics for yield modeling. *Ecol. Indic.* **121**, 107124 (2021).

68. Pourzand, F., Noy, I. & Sağlam, Y. Droughts and farms' financial performance: a farm-level study in New Zealand. *Aust. J. Agric. Resour. Econ.* **64**, 818–844 (2020).

Acknowledgements

We are grateful for the Whakahura Endeavour program (New Zealand Ministry for Business, Innovation, and Employment) for funding this research

Author contribution statement

Elodie Blanc processed the data, contributed to the statistical analysis of the data, wrote the description of the methodology and data, and prepared the figures. Ilan Noy wrote the main manuscript text and contributed to the statistical analysis. All authors reviewed the manuscript.

Data availability statement

All data are available upon request.

Competing Interests statement

None.

Figures

Figure 1. Examples of land use for primary parcels (Waimakariri and Selwyn districts, Canterbury)

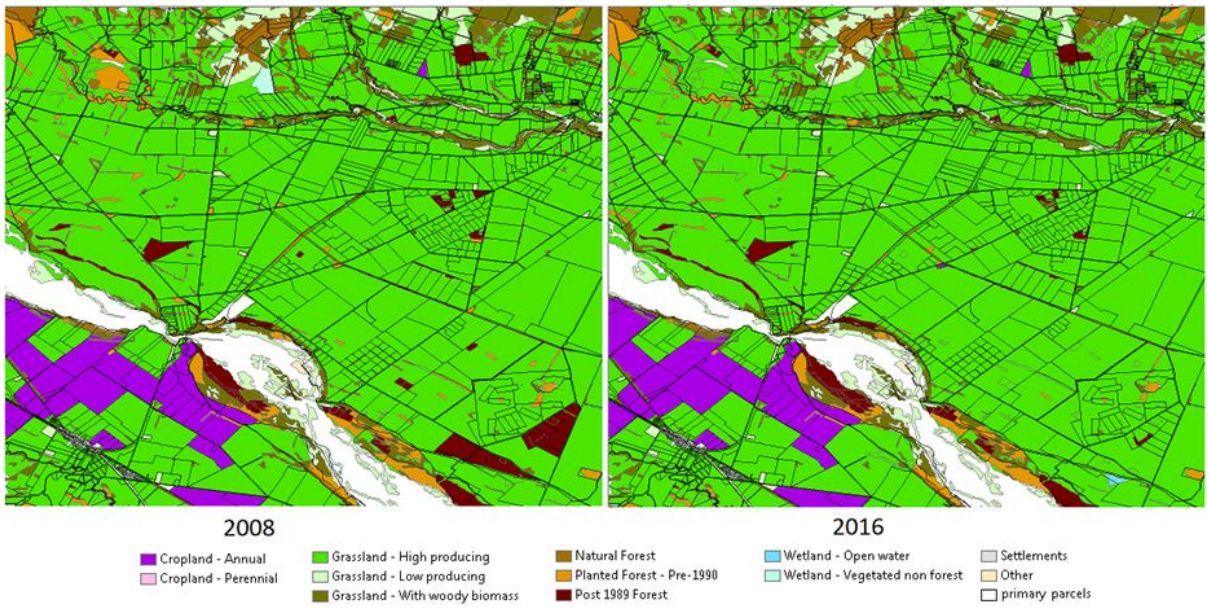

Figure 2. Example of EVI and primary parcels (02/02/2010; Waimakariri and Selwyn districts, Canterbury)

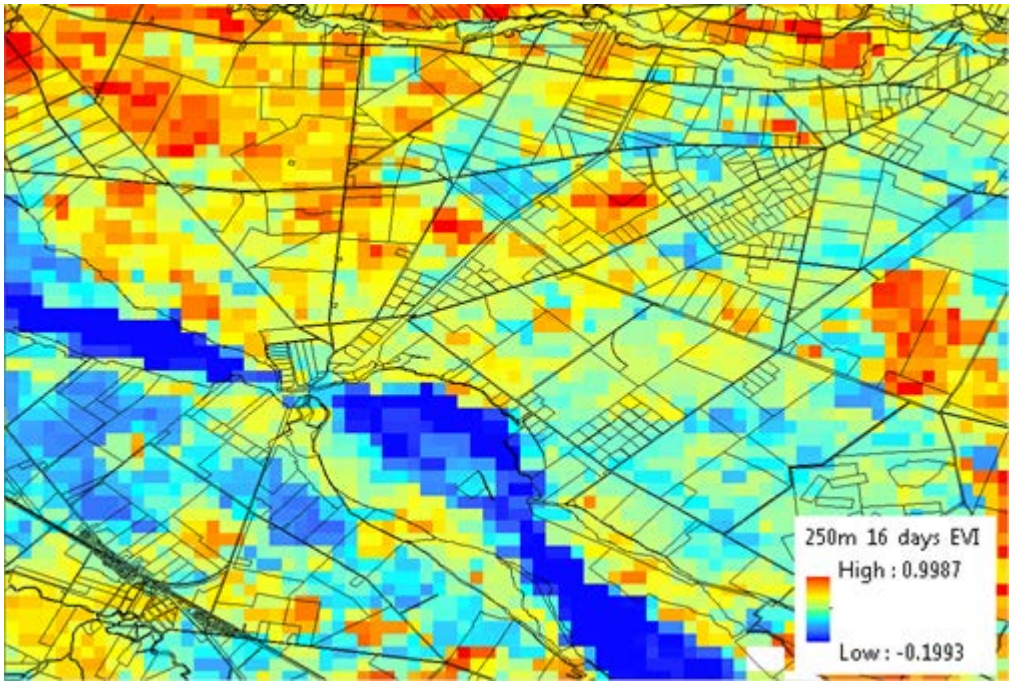

Figure 3. Illustration of the drought and flood duration and magnitude

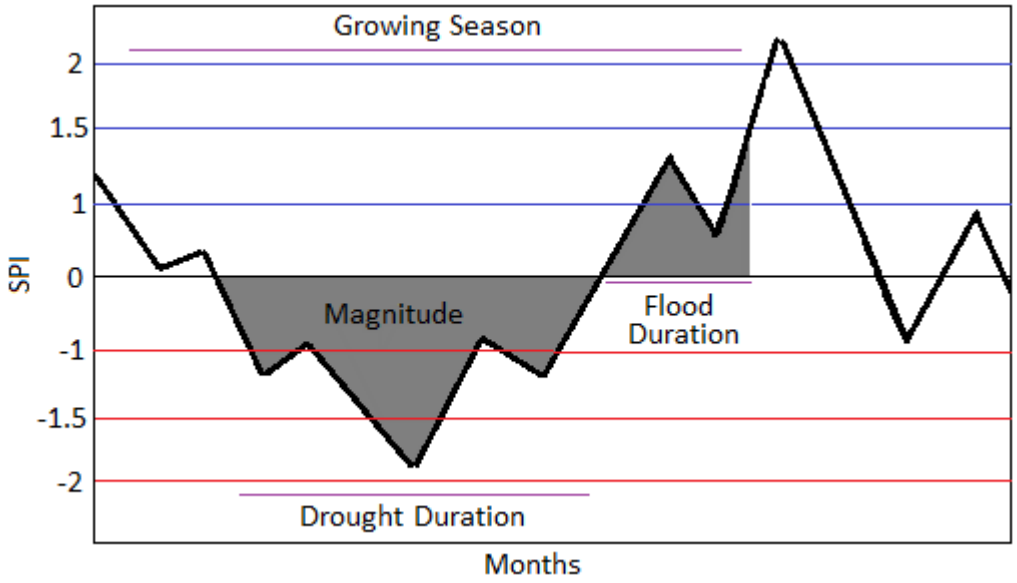

Figure 4. Flood return interval

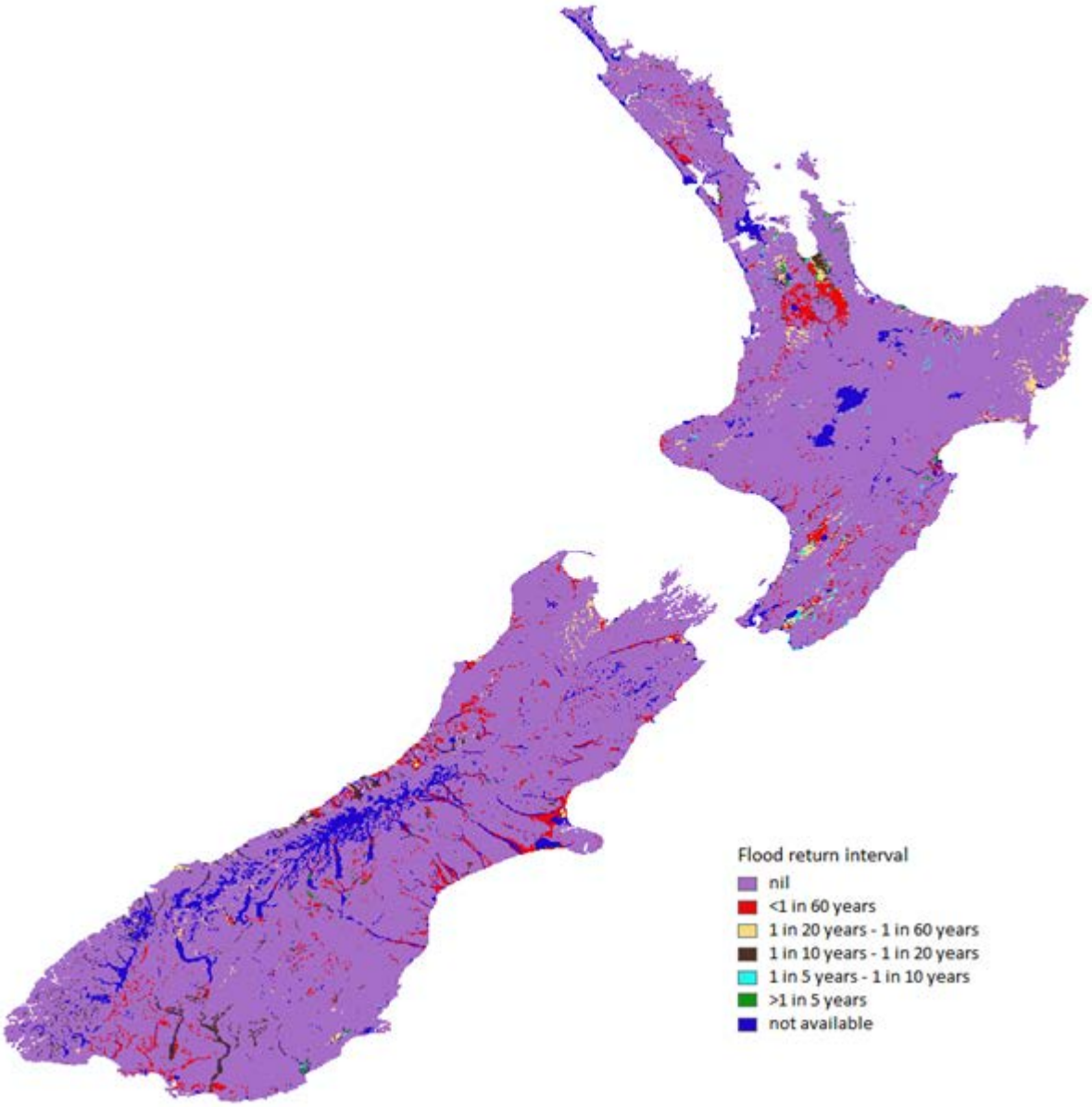

Figure 5. Box plot of impacts (excluding outsiders) on annual crops

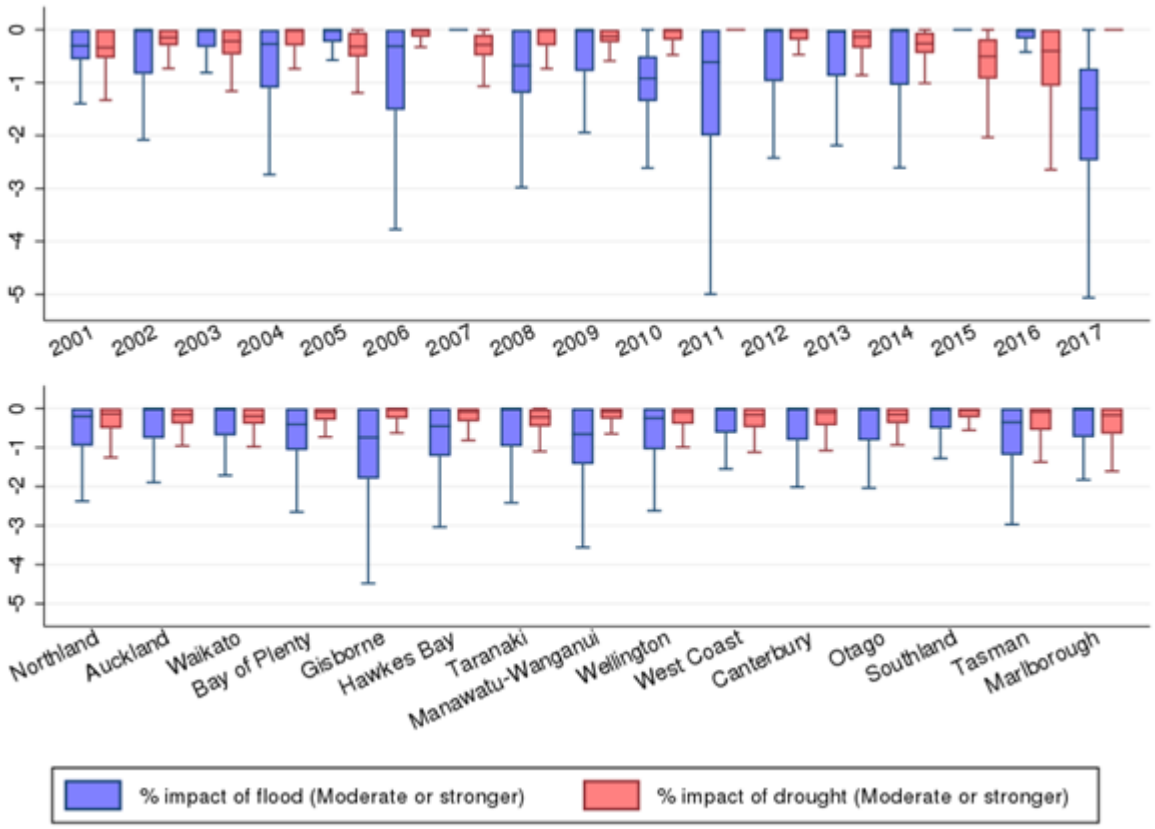

Figure 6. Box plot of impacts (excluding outsiders) on perennial crops

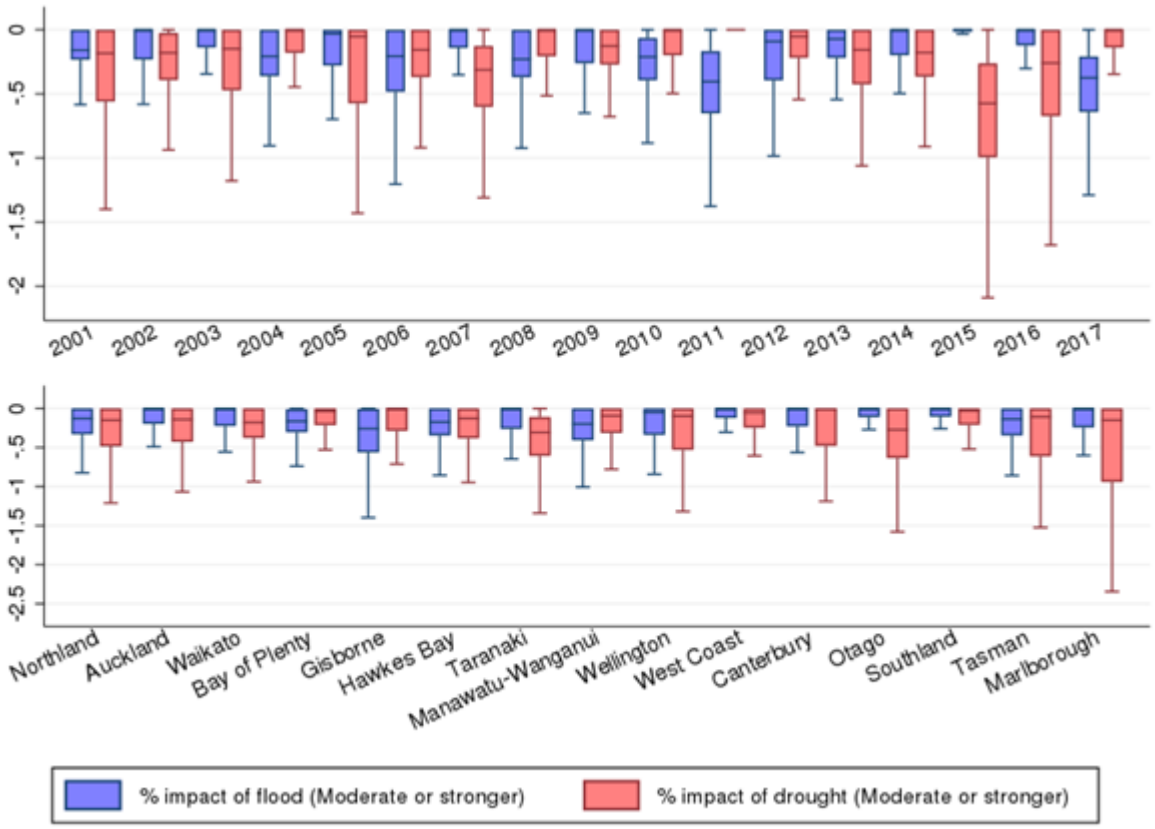

Figure 7. Average impact (2001-2017) on annual crops

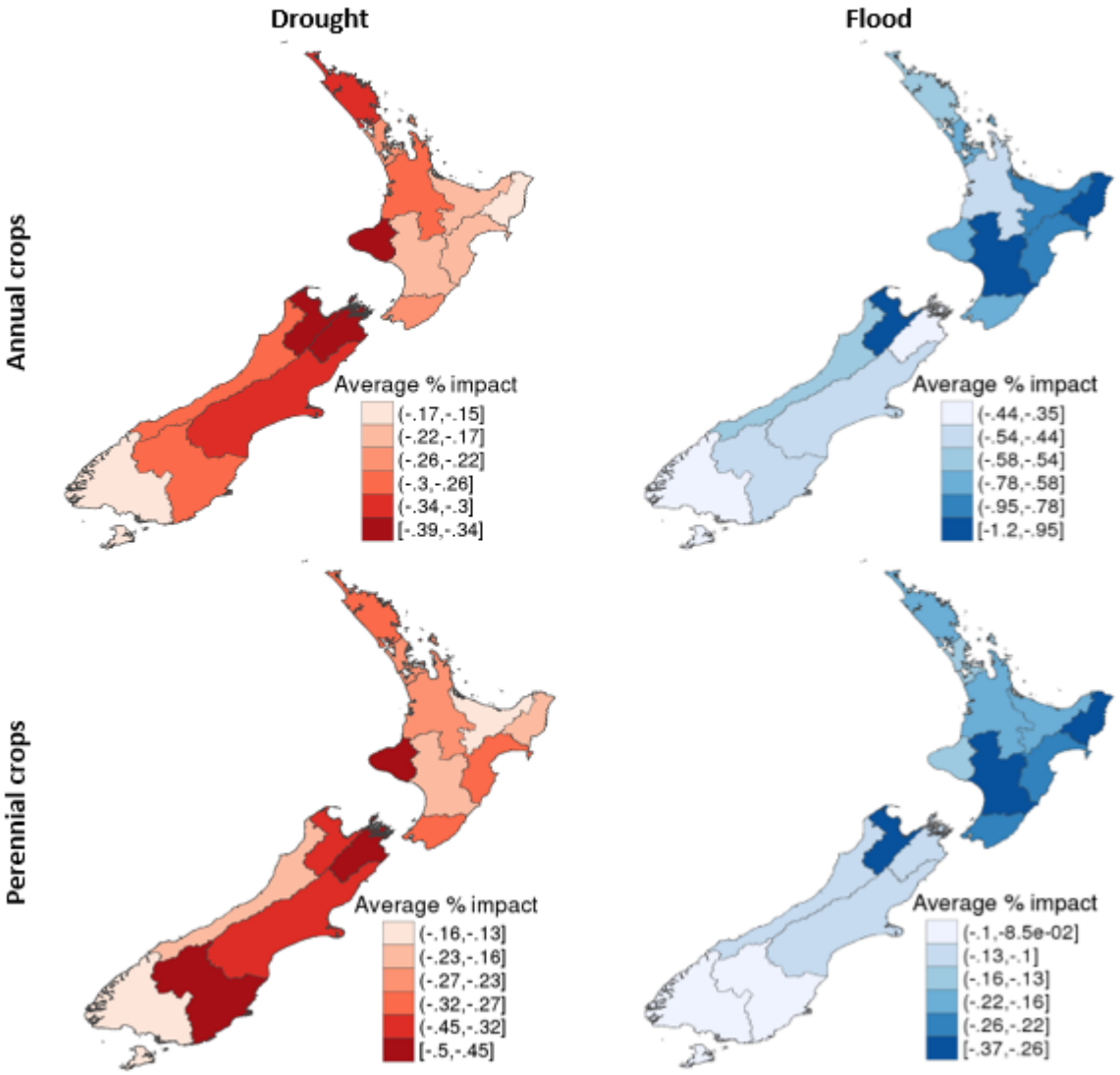

Figure 8. Box plot of impacts (excluding outsiders) on low-producing pasture

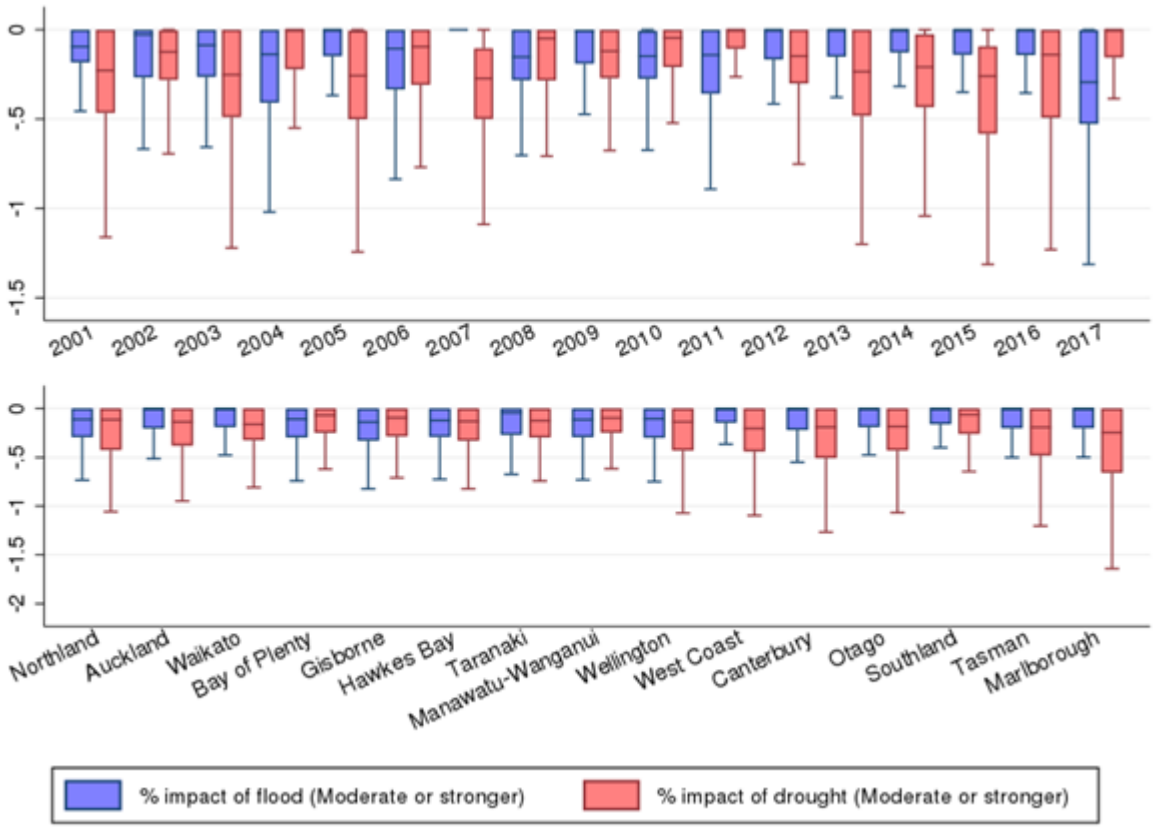

Figure 9. Box plot of impacts (excluding outsiders) on pasture with woody biomass

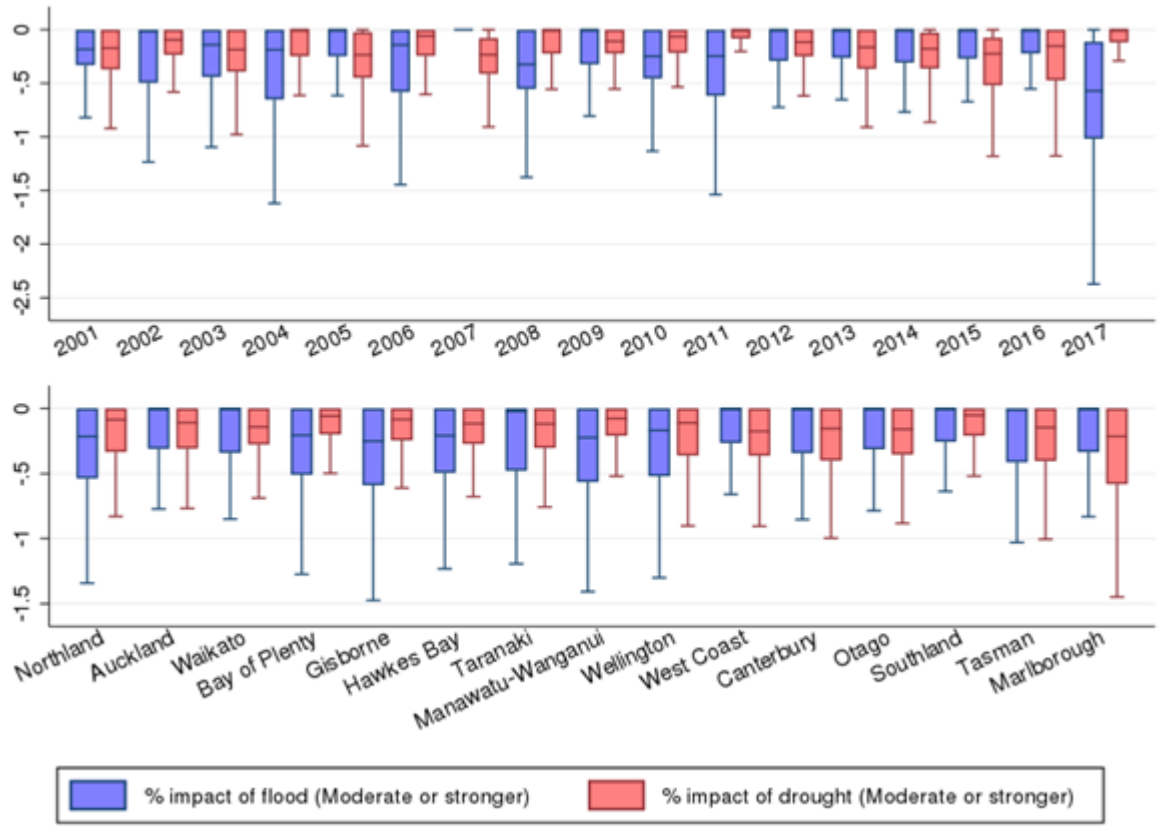

Figure 10. Box plot of impacts (excluding outsiders) on high-producing pasture

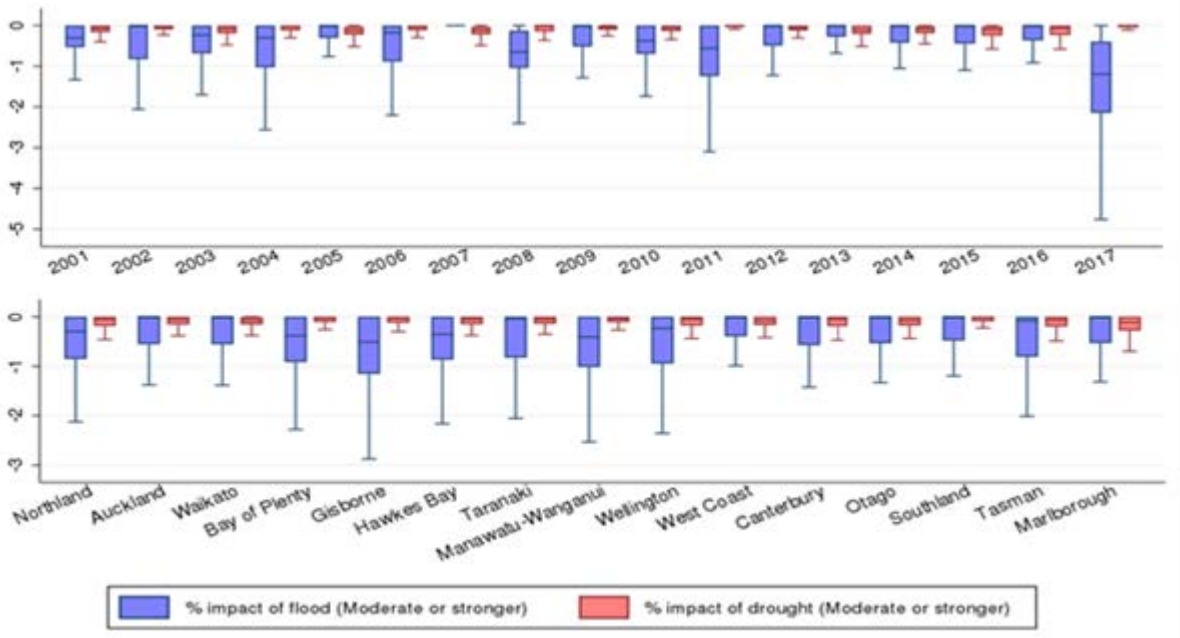

Figure 11. Average impact (2001-2017) on pasture

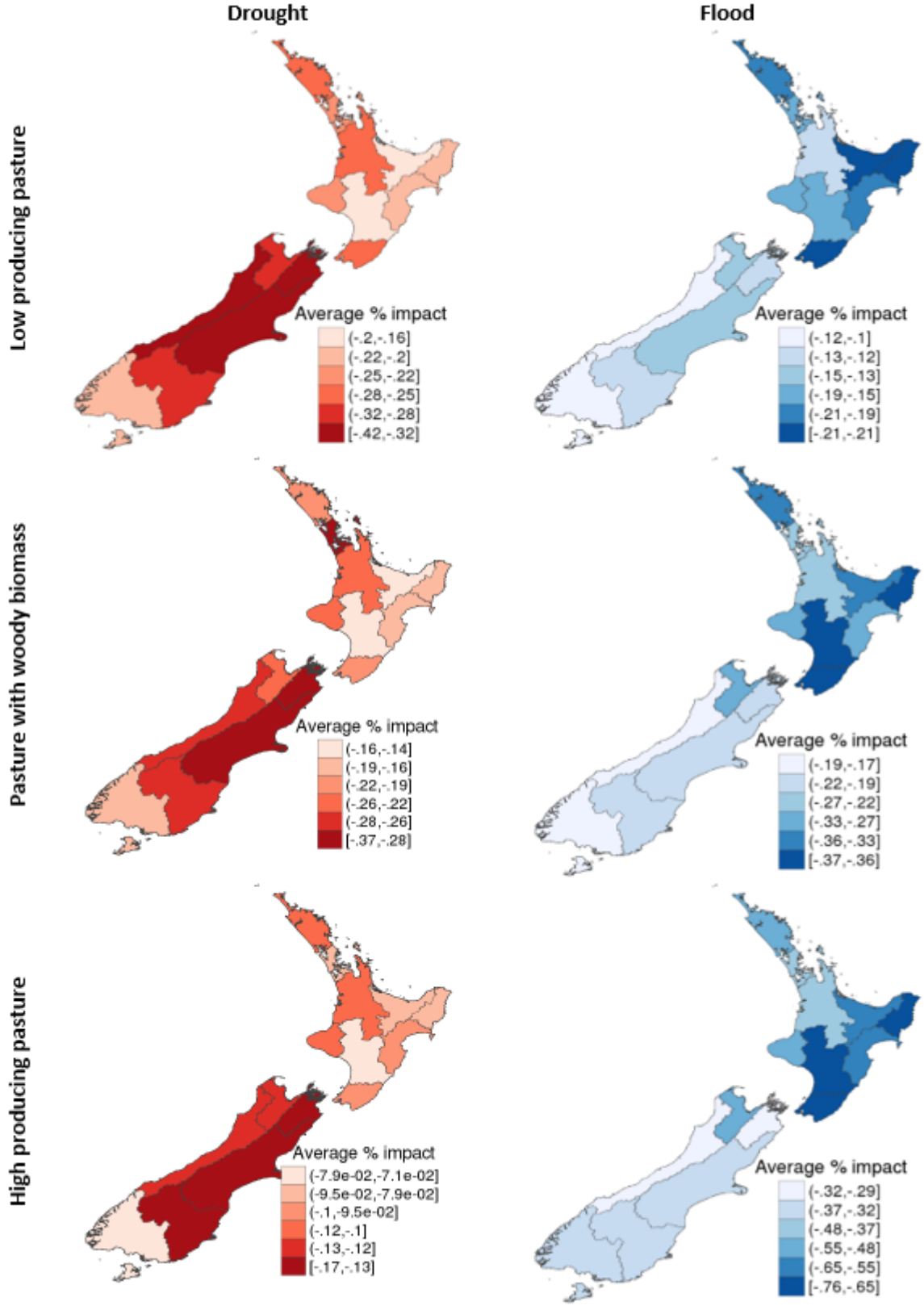

Tables

Table 1. Variable descriptions

Variable	Description
Tmin	Minimum diurnal temperature
Tmax	Maximum diurnal temperature
GSL	Growing season length
modD+ M	Moderate or stronger drought magnitude
modF+ M	Moderate or stronger flood magnitude
sevD+ M	Severe or stronger drought magnitude
sevF+ M	Severe or stronger flood magnitude
extD+ M	Extreme or stronger drought magnitude
extF+ M	Extreme or stronger flood magnitude
rf2345	Zone with flood return interval of category 2, 3,4 or 5
rf1	Zone with flood return interval of category 1 (Nil)

Table 2. Descriptive statistics for crops

	Variables	Mean	Std. Dev.	Min	Max
Annual (748,413 obs)	maxEVI	.608	.098	.007	.997
	Tmin	8.131	2.651	-2.93	16.795
	Tmax	18.013	2.216	6.284	25.768
	GSL	190.142	55.568	43	362
	mod+D M	.029	.044	0	1.283
	mod+F M	.021	.033	0	.479
	sev+D M	.023	.044	0	1.283
	sev+F M	.015	.032	0	.479
	ext+D M	.016	.042	0	1.283
	ext+F M	.009	.029	0	.479
	rf2345	.329	.47	0	1
	rf1	.653	.476	0	1
Perennial (522,483 obs)	maxEVI	.601	.088	-.073	.99
	Tmin	9.411	2.36	-1.941	16.933
	Tmax	19.012	1.875	8.119	25.768
	GSL	214.873	61.863	48	357
	mod+D M	.024	.037	0	1.331
	mod+F M	.023	.032	0	.51
	sev+D M	.02	.037	0	1.331
	sev+F M	.019	.033	0	.51
	ext+D M	.013	.034	0	1.331
	ext+F M	.01	.028	0	.51
	rf2345	.272	.445	0	1
	rf1	.717	.45	0	1

Table 3. Descriptive statistics for pasture

	Variables	Mean	Std. Dev.	Min	Max
Low producing pasture (2,770,211 obs)	maxEVI	.571	.114	-.113	.999
	Tmin	7.044	2.506	-5.876	17.753
	Tmax	17.001	2.125	-.227	25.327
	GSL	220.051	53.235	40	366
	mod+D M	.027	.039	0	1.372
	mod+F M	.019	.03	0	.936
	sev+D M	.022	.04	0	1.372
	sev+F M	.015	.03	0	.936
	ext+D M	.014	.037	0	1.372
	ext+F M	.008	.027	0	.936
	rf2345	.132	.338	0	1
	rf1	.727	.446	0	1
Pasture with woody biomass (2,817,577 obs)	maxEVI	.602	.102	-.068	.999
	Tmin	7.374	2.547	-4.41	17.755
	Tmax	17.162	2.085	1.401	25.289
	GSL	215.867	55.048	42	362
	mod+D M	.027	.039	0	1.388
	mod+F M	.02	.031	0	.603
	sev+D M	.022	.04	0	1.388
	sev+F M	.015	.031	0	.603
	ext+D M	.014	.038	0	1.388
	ext+F M	.009	.027	0	.603
	rf2345	.166	.372	0	1
	rf1	.786	.41	0	1
High producing pasture (9,838,844 obs)	maxEVI	.644	.085	-.115	1
	Tmin	7.854	2.445	-3.952	17.759
	Tmax	17.451	2.056	2.052	25.332
	GSL	206.806	57.075	40	362
	mod+D M	.027	.04	0	1.372
	mod+F M	.021	.033	0	.631
	sev+D M	.023	.04	0	1.372
	sev+F M	.016	.033	0	.631
	ext+D M	.015	.038	0	1.372
	ext+F M	.009	.03	0	.631
	rf2345	.253	.435	0	1
	rf1	.735	.441	0	1

Table 4. Regression results for annual crops

Variables	(1) Moderate	(2) Moderate, flood zones	(3) Severe	(4) Severe, flood zones	(5) Extreme	(6) Extreme, flood zones
Tmin	0.00191***	0.00190***	0.00149***	0.00143***	0.000780	0.000780
Tmin2	0.000561***	0.000561***	0.000570***	0.000573***	0.000606***	0.000606***
Tmax	0.0644***	0.0644***	0.0654***	0.0655***	0.0673***	0.0673***
Tmax2	-0.00194***	-0.00195***	-0.00197***	-0.00197***	-0.00202***	-0.00202***
mod+D M	-0.0539***	-0.0538***				
mod+F M	-0.179***	-0.178***				
mod+F M x rf2345		-0.00402				
sev+D M			-0.0476***	-0.0475***		
sev+F M			-0.144***	-0.135***		
sev+F M x rf2345				-0.0235***		
ext+D M					-0.0507***	-0.0507***
ext+F M					-0.155***	-0.155***
ext+F M x rf2345						0.000195
Constant	0.0375***	0.0374***	0.0272***	0.0263***	0.0115	0.0115
Observations	748,413	748,413	748,413	748,413	748,413	748,413
Number of id	40,294	40,294	40,294	40,294	40,294	40,294
R2 within	0.04012	0.0401	0.03830	0.0383	0.03830	0.0383
R2 between	0.02799	0.0280	0.02708	0.0273	0.02840	0.0284
R2 overall	0.00001	9.71e-06	0.00001	1.17e-05	0.00002	2.49e-05
RMSE	0.06707	0.0671	0.06714	0.0671	0.06714	0.0671

Notes: Robust standard errors in parentheses; *** p<0.01, ** p<0.05, * p<0.1;

Table 5. Regression results for perennial crops

Variables	(1) Moderate	(2) Moderate, flood zones	(3) Severe	(4) Severe, flood zones	(5) Extreme	(6) Extreme, flood zones
Tmin	0.000335	0.000306	0.000353	0.000317	0.000951*	0.000954*
Tmin2	0.000642***	0.000640***	0.000637***	0.000634***	0.000649***	0.000650***
Tmax	0.0678***	0.0677***	0.0678***	0.0677***	0.0680***	0.0680***
Tmax2	-0.00202***	-0.00202***	-0.00202***	-0.00202***	-0.00205***	-0.00205***
mod+D M	-0.0643***	-0.0641***				
mod+F M	-0.0524***	-0.0404***				
mod+F M x rf2345		-0.0331***				
sev+D M			-0.0609***	-0.0610***		
sev+F M			-0.0378***	-0.0203***		
sev+F M x rf2345				-0.0484***		
ext+D M					-0.0622***	-0.0621***
ext+F M					-0.0868***	-0.0890***
ext+F M x rf2345						0.00593
Constant	-0.0108	-0.0102	-0.0123	-0.0116	-0.0144	-0.0145
Observations	522,483	522,483	522,483	522,483	522,483	522,483
Number of id	31,346	31,346	31,346	31,346	31,346	31,346
R2 within	0.03882	0.0389	0.03863	0.0388	0.04008	0.0401
R2 between	0.10425	0.106	0.10449	0.107	0.10190	0.102
R2 overall	0.09316	0.0946	0.09310	0.0951	0.09225	0.0921
RMSE	0.04923	0.0492	0.04923	0.0492	0.04920	0.0492

Table 6. Regression results for low-producing pasture

Variables	(1) Moderate	(2) Moderate, flood zones	(3) Severe	(4) Severe, flood zones	(5) Extreme	(6) Extreme, flood zones
Tmin	0.00890***	0.00890***	0.00886***	0.00885***	0.00876***	0.00875***
Tmin2	-0.000115***	-0.000115***	-0.000116***	-0.000116***	-0.000112***	-0.000112***
Tmax	0.0205***	0.0205***	0.0206***	0.0206***	0.0207***	0.0207***
Tmax2	-0.000610***	-0.000610***	-0.000611***	-0.000611***	-0.000614***	-0.000614***
mod+D M	-0.0523***	-0.0524***				
mod+F M	-0.0451***	-0.0379***				
mod+F M x rf2345		-0.0524***				
sev+D M			-0.0465***	-0.0466***		
sev+F M			-0.0317***	-0.0229***		
sev+F M x rf2345				-0.0650***		
ext+D M					-0.0437***	-0.0438***
ext+F M					-0.0151***	-0.00181
ext+F M x rf2345						-0.0958***
Constant	0.348***	0.348***	0.347***	0.347***	0.345***	0.345***
Observations	2,770,211	2,770,211	2,770,211	2,770,211	2,770,211	2,770,211
Number of id	146,031	146,031	146,031	146,031	146,031	146,031
R2 within	0.04281	0.0429	0.04258	0.0427	0.04230	0.0425
R2 between	0.00627	0.00617	0.00641	0.00629	0.00625	0.00614
R2 overall	0.03483	0.0348	0.03506	0.0350	0.03479	0.0348
RMSE	0.05222	0.0522	0.05223	0.0522	0.05224	0.0522

Table 7.Regression results for pasture with woody biomass

Variables	(1) Moderate	(2) Moderate, flood zones	(3) Severe	(4) Severe, flood zones	(5) Extreme	(6) Extreme, flood zones
Tmin	0.00976***	0.00975***	0.00964***	0.00964***	0.00953***	0.00954***
Tmin2	-0.000158***	-0.000157***	-0.000156***	-0.000156***	-0.000153***	-0.000153***
Tmax	0.0209***	0.0209***	0.0211***	0.0211***	0.0213***	0.0213***
Tmax2	-0.000616***	-0.000616***	-0.000620***	-0.000621***	-0.000625***	-0.000626***
mod+D M	-0.0457***	-0.0455***				
mod+F M	-0.0816***	-0.0701***				
mod+F M x rf2345		-0.0593***				
sev+D M			-0.0340***	-0.0339***		
sev+F M			-0.0588***	-0.0477***		
sev+F M x rf2345				-0.0576***		
ext+D M					-0.0336***	-0.0336***
ext+F M					-0.0425***	-0.0315***
ext+F M x rf2345						-0.0556***
Constant	0.368***	0.368***	0.365***	0.365***	0.363***	0.363***
Observations	2,817,577	2,817,577	2,817,577	2,817,577	2,817,577	2,817,577
Number of id	162,348	162,348	162,348	162,348	162,348	162,348
R2 within	0.05334	0.0535	0.05237	0.0525	0.05181	0.0519
R2 between	0.00115	0.000992	0.00133	0.00119	0.00141	0.00134
R2 overall	0.01954	0.0191	0.01982	0.0195	0.01989	0.0197
RMSE	0.04782	0.0478	0.04785	0.0478	0.04786	0.0479

Table 8. Regression results for high producing pasture

Variables	(1) Moderate	(2) Moderate, flood zones	(3) Severe	(4) Severe, flood zones	(5) Extreme	(6) Extreme, flood zones
Tmin	0.00928***	0.00928***	0.00930***	0.00930***	0.00931***	0.00931***
Tmin2	-0.000197***	-0.000198***	-0.000204***	-0.000204***	-0.000208***	-0.000208***
Tmax	0.0240***	0.0240***	0.0242***	0.0242***	0.0244***	0.0245***
Tmax2	-0.000709***	-0.000709***	-0.000713***	-0.000713***	-0.000720***	-0.000721***
mod+D M	-0.0240***	-0.0239***				
mod+F M	-0.147***	-0.132***				
mod+F M x rf2345		-0.0573***				
sev+D M			-0.0111***	-0.0111***		
sev+F M			-0.122***	-0.106***		
sev+F M x rf2345				-0.0594***		
ext+D M					-0.0146***	-0.0146***
ext+F M					-0.120***	-0.104***
ext+F M x rf2345						-0.0570***
Constant	0.387***	0.387***	0.384***	0.384***	0.381***	0.381***
Observations	9,838,844	9,838,844	9,838,844	9,838,844	9,838,844	9,838,844
Number of id	480,723	480,723	480,723	480,723	480,723	480,723
R2 within	0.04269	0.0429	0.04064	0.0409	0.03961	0.0398
R2 between	0.00827	0.00833	0.00825	0.00829	0.00811	0.00815
R2 overall	0.00131	0.00131	0.00108	0.00109	0.00100	0.00100
RMSE	0.05018	0.0502	0.05023	0.0502	0.05026	0.0503

Table A1. Variable definitions

Variable	Description
tmean	Mean diurnal temperature
tmin	Minimum diurnal temperature
tmax	Maximum diurnal temperature
tminFP1	Fractional polynomial term 1 of minimum diurnal temperature
tminFP2	Fractional polynomial term 2 of minimum diurnal temperature
tmaxFP1	Fractional polynomial term 1 of maximum diurnal temperature
tmaxFP2	Fractional polynomial term 2 of maximum diurnal temperature
modD+ dum	Moderate or stronger drought dummy
modF+ dum	Moderate or stronger flood dummy
sevD+ dum	Severe or stronger drought dummy
sevF+ dum	Severe or stronger flood dummy
extD+ dum	Extreme or stronger drought dummy
extF+ dum	Extreme or stronger flood dummy
modD dum	Moderate drought dummy
modF dum	Moderate flood dummy
sevD dum	Severe drought dummy
sevF dum	Severe flood dummy
extD dum	Extreme drought dummy
extF dum	Extreme flood dummy
modD L	Moderate drought length
modF L	Moderate flood length
sevD L	Severe drought length
sevF L	Severe flood length
extD L	Extreme drought length
extF L	Extreme flood length
modD M	Moderate drought magnitude
modF M	Moderate flood magnitude
sevD M	Severe drought magnitude
sevF M	Severe flood magnitude
extD M	Extreme drought magnitude
extF M	Extreme flood magnitude

Table A2. Descriptive statistics for crops

	Variables	Mean	Std. Dev.	Min	Max
Annual (748,413 obs)	Tmin	8.131	2.651	-2.93	16.795
	Tmax	18.013	2.216	6.284	25.768
	GSL	190.142	55.568	43	362
	modD M	.006	.015	0	.616
	modF M	.005	.014	0	.245
	sevD M	.007	.02	0	.616
	sevF M	.007	.019	0	.314
	extD M	.016	.042	0	1.283
	extF M	.009	.029	0	.479
	rf2345	.329	.47	0	1
	rf1	.653	.476	0	1
Perennial (522,483 obs)	Tmin	9.411	2.36	-1.941	16.933
	Tmax	19.012	1.875	8.119	25.768
	GSL	214.873	61.863	48	357
	modD M	.004	.013	0	.269
	modF M	.004	.011	0	.245
	sevD M	.007	.02	0	.432
	sevF M	.009	.021	0	.314
	extD M	.013	.034	0	1.331
	extF M	.01	.028	0	.51
	rf2345	.272	.445	0	1
	rf1	.717	.45	0	1

Table A3. Descriptive statistics for pasture

	Variables	Mean	Std. Dev.	Min	Max
Low producing pasture (2,770,211 obs)	Tmin	7.044	2.506	-5.876	17.753
	Tmax	17.001	2.125	-.227	25.327
	GSL	220.051	53.235	40	366
	modD M	.005	.013	0	.572
	modF M	.004	.011	0	.465
	sevD M	.008	.02	0	.572
	sevF M	.007	.018	0	.465
	extD M	.014	.037	0	1.372
	extF M	.008	.027	0	.936
	rf2345	.132	.338	0	1
	rf1	.727	.446	0	1
Pasture with woody biomass (2,817,577 obs)	Tmin	7.374	2.547	-4.41	17.755
	Tmax	17.162	2.085	1.401	25.289
	GSL	215.867	55.048	42	362
	modD M	.005	.014	0	.651
	modF M	.005	.011	0	.363
	sevD M	.008	.021	0	.763
	sevF M	.007	.018	0	.432
	extD M	.014	.038	0	1.388
	extF M	.009	.027	0	.603
	rf2345	.166	.372	0	1
	rf1	.786	.41	0	1
High producing pasture (9,838,844 obs)	Tmin	7.854	2.445	-3.952	17.759
	Tmax	17.451	2.056	2.052	25.332
	GSL	206.806	57.075	40	362
	modD M	.005	.014	0	.681
	modF M	.005	.012	0	.465
	sevD M	.008	.021	0	.856
	sevF M	.007	.018	0	.465
	extD M	.015	.038	0	1.372
	extF M	.009	.03	0	.631
	rf2345	.253	.435	0	1
	rf1	.735	.441	0	1